The 4th IEEE International Conference on E-Health and Bioengineering - EHB 2013
Grigore T. Popa University of Medicine and Pharmacy, Iaşi, Romania, November 21-23, 2013

Handheld Surgical Drill With Integrated Thrust Force Recognition

Markus Hessinger, Jürgen Hielscher, Peter P. Pott, Roland Werthschützky
Institut für Elektromechanische Konstruktionen
Technische Universität Darmstadt
Darmstadt, Germany

Abstract - Spine surgeries are particularly high-risk procedures with the imminent danger of spinal cord and blood vessel injuries. High accuracy and safety are important aspects in the use of medical devices during invasive interventions. For exact positioning of the drill hole, drill tip pose recognition and bone layer breakthrough detection is required.
This paper presents a concept design and first results of a novel navigated handheld surgical device for bone drilling with integrated thrust force sensing and active optical markers for real-time pose recognition. The developed force sensor measures the applied thrust force on the drill tip with a cylindrical deformation element, integrated between the axial bearing of the shaft and the casing. The deflection of the deformation element is acquired by bonded resistive strain gauges. First experiments show sufficient results of the thrust force resolution for breakthrough detection.

Keywords: Navigation, surgical drill, thrust force sensor, handheld device, sensor integration

I. INTRODUCTION

Medical robotics has been an integral part in engineering and medical research for the past decades. While the goal of industrial robotics is to replace the employment of human workers for recurring tasks, medical robots aim to work in cooperation with the surgeon. A medical robot combines the abilities of humans to make decisions and to control the robots with prior anatomical knowledge with its precision and repeatability. This leads to higher accuracy during operation with the benefit of rapid recovery. Highly invasive procedures like drilling in bones require careful handling of the surgical tools. A typical example for a high-risk procedure in orthopedic surgery is the pedicle screw insertion in spine surgery, where little deviations between the planned and executed drilling path can cause irreversible damage to the human body. The main challenge during the operation is to place the screws in the angular axis of the pedicle due to variable anatomy of vertebral body and relatively small pedicle diameter in thoracic vertebra [1]. Inaccurate placement can lead to pedicle fractures and vascular damage or injure the central nervous system. There are two critical phases during the drilling process: (1) The drill tip must be placed in the correct position and angle on the pedicle of the vertebral arch, consisting of hard cortical bone. (2) The feed rate of the drill must stop behind the transition of the less dense cancellous bone in the cortical rim to avoid a breakthrough. The reliability of the procedure depends on the surgeon's haptic and visual sensing as well as the general clinical experience. A robotic system is capable to feedback sensing data of the operation state to support the surgeon's decisions. Some drilling parameters, such as drilling torque and rotational speed, are simple to measure, while measuring thrust force or drill position requires additional sensors which must be integrated into the drill system. The procedure of pedicle screw placement is currently performed with a conventional surgical drill under visual assessment and radiologic control. Studies under clinical conditions have shown the effectiveness of computer assistance in pedicle screw insertions during spinal surgery [2]. Several research projects are based on the field of computer-assisted orthopedic surgery with the focus on pedicle screw fixation in spinal surgery [3-11], where surgical tools are bone-mounted [3], connected to industrial robots [5] or mounted on specially designed robot arms [10]. Their field of application varies from positioning, drilling or telesurgical tasks. However, large robotic systems for orthopedic surgery are very cost ineffective and require training and maintenance. A different approach in surgical robotic systems focuses on small, handheld devices developed specially for increased convenience during operation [12]. Several studies deal with sensing thrust force to establish technical parameters of the drilling process [13-15]. The main feature is the state recognition of the drilling bit in different bone layers for breakthrough detection. With the knowledge of the bone's composition, the depth of the drilled screw path can be obtained and bone overheating can be avoided. ODRO is a handheld robotized system for bone drilling manipulations with integrated breakthrough detection [14]. The surgical device monitors depth of penetration of the drill by measuring the thrust force between drill motor and casing. Position and orientation of the tip during the drilling process is not verified.

In this paper, a compact handheld surgical drill is proposed. A thrust force sensor and an active infrared LED marker are integrated into the portable device in order to enable high accuracy during pedicle screw positioning without permanent X-radiation exposure. The sensor is designed to measure the axial thrust force of the drill bit without transverse forces. For this reason, the deformation element is included next to the

978-1-4799-2373-1/13/$31.00 ©2013 IEEE

rotating shaft of the drill with no requirements of extra space. The aim of this paper is to show the process in its entirety, from designing a surgical device, to the construction and integration of a force sensor up to its simulation, completion and evaluation in first testing scenarios.

II. Design of the Handheld Drill Device

A. Basic design approaches

The drill device is developed to support the surgeon with real-time data of the drill tip position, orientation and thrust force during operation. The body has a cylindrical shape of 150 mm length and 24 mm diameter to fit in the hand of the surgeon. For weight reducing purpose, the drill actuation motor is placed outside the device and connected via flex-shaft to the rotation shaft. For real-time navigation and position feedback of the drill, an optical tracking system (accuTrack 250, Atracsys LLC, Le Mont-sur-Lausanne, Switzerland) is used. The designed marker consists of six IR LEDs, oriented in two triangles with 90° displacement. The integrated marker array covers a radiation angle of 210° along the rotation axis (see figure 1). With the offset arrangement of the LEDs in three dimensions of the Cartesian coordinates, a position determination with the precision of 0.1 mm is possible. The active IR LEDs are currently sampled with 1.5 kHz for optimal speed/accuracy ratio. The navigation system, consisting of the tool marker with six LEDs and patient marker with four LEDs, reaches a sampling frequency of 150 Hz for an accurate detection of fast movements of the device.

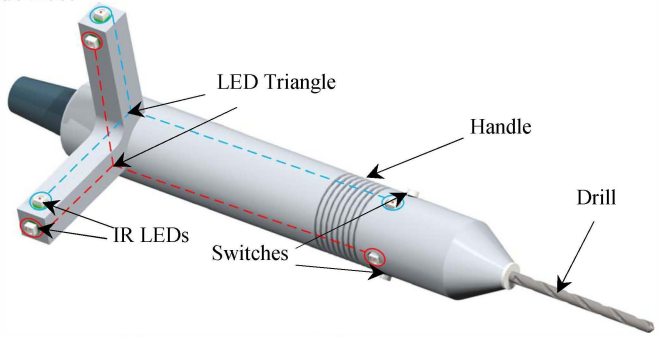

Fig 1. Design of the handheld drill device

B. Integration of force sensing

The motivation of integrating a force sensor into the drill device is based on two reasons: (1) Reducing extra space which is required to attach an external force sensor into the force flux of the drill system. (2) Improving the force sensor resolution by measuring the thrust force in one dimension directly at the shaft of the drill bit. Flexible parts of the casing or drill motor have no influence on the force signal.

The average thrust force during the drill process is 8 N in hard bone layer [16]. Various physical principles are possible to measure the thrust force of the drill. Considering the requirements of a quasistatic measuring process and a compact structure let the elastic deformation with a resistive measurement principle be rated best.

The integration of the force sensor comes with several challenges. Since the sensor cannot be integrated into the rotation shaft, it must be connected to the axially movable radial bearing on the one side and to the fixed inner casing on the other. This limits the dimensions of the cylindrical deformation body to 11 mm external and 9 mm internal diameter. The height of the body is chosen to 25 mm to enable access to the flexure beam to place the strain gauges. Figure 2 shows the integration of the force sensor into the mechanical structure of the device. The axial force F_z causes a compression of the deformation element ξ. The consequential strain and compression on the flexure beam is detected by strain gauges (see figure 3(c)). The shear forces F_x and F_y are compensated by the radial bearing. Oil lubrication between the radial bearing and brass casing decreases friction in axial direction.

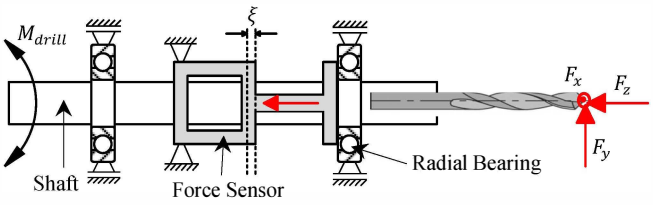

Fig 2. Mechanical structure with force sensor integration

C. Dimensioning of the deformation body

The shape of the element is shown in figure 3(a). The vertical beams for the application of the force on the flexure beam have a thickness of 1 mm to enable a maximal surface for the strain. The measuring range is limited to 20 N with an overload tolerance of factor 4. The deformation of the element under various loads is simulated with FEM analysis software (ANSYS, Inc.). For an overload of 80 N, the tensile strength of the construction steel (S275JR) of 275 N/mm^2 may not be exceeded. Notch stress in the vertical edges is reduced by adding a radius of 0.5 mm to the transition between the vertical and horizontal beam.

Taking maximal strain and overload tolerance into account, the thickness of the flexure beam is optimized to 700 µm, with an average of 0.4 mm/m strain at maximum stress position and an axial deformation of 15.14 µm. Figure 3(b) shows the strain over the flexure beam under load.

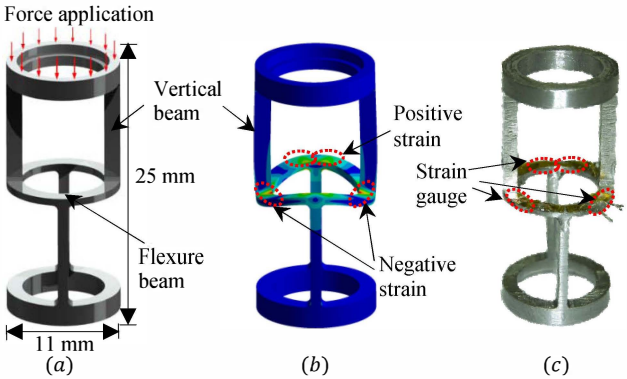

Fig 3. Deformation body: (a) First CAD design, (b) FEM simulation of strain characteristics, (c) Structural steel element with strain gauges.

The optimal placement of the strain gauges at maximal strain and compression is analyzed with the strain characteristics of a cylindrical path on the flexure beam (figure 4). The meander of the strain gauge is placed on the position of maximal strain. Since the maximal compression is located on the stress compensation radius, the strain gauge must be placed as close as possible to it. Strain gauge with 0.3 mm grid length, 0.9 mm grid width and 120 Ω (type 1-LY11-0.3/120, HBM Inc.) are bonded on the flexure beam and contacted via thin enameled wire.

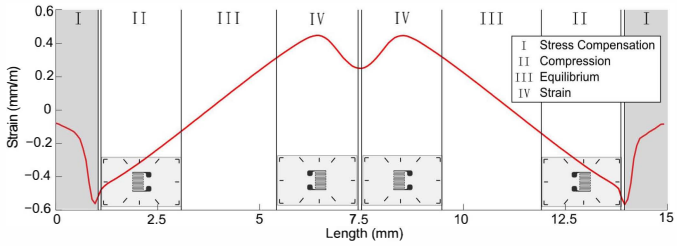

Fig 4. Strain over flexure beam length with strain gauge placement

Figure 3(c) shows the deformation body with four strain gauges. The maximal compression of the deformation element of 15.13 µm is acquired by the resistance strain gauges which are wired to a full bridge, where two strain gauges measure strain and two strain gauges compression, respectively. Strain gauges and copper wire are protected from mechanical stress with an applied silicone layer.

The manufacturing of the deformation element with a weight of 2 g is time consuming and thus cost expensive. A new approach is tested by using a 3D printed deformation body with an alloy of 70 % steel and 30 % bronze that costs less than 10 € in production. Although little manufacturing defects occur with the 3D printing method, the deformation element meets the requirements of size and surface condition.

The linearity behavior between applied force and measured bridge voltage of both elements is investigated in the following paragraph.

III. Force Sensor Evaluation

A. *Sensor calibration*

The force/voltage response characteristics of the developed force sensor are evaluated with a sensor calibration setup as show in figure 5. At first, the two force sensors with the manufactured and sintered deformation element are fixed between a force transducer load cell (Type U1A, HBM, Germany) and the table. The load cell is moved by a linear drive to compress and decompress the sensor. The load cell is readout with a bridge amplifier (Type MC 30, HBM Inc.) and the full bridge circuit of the sensor is readout by a bridge amplifier (Type 5271, Kistler Instrumente AG, Germany) with 5 V bridge voltage and an amplification factor of 200.

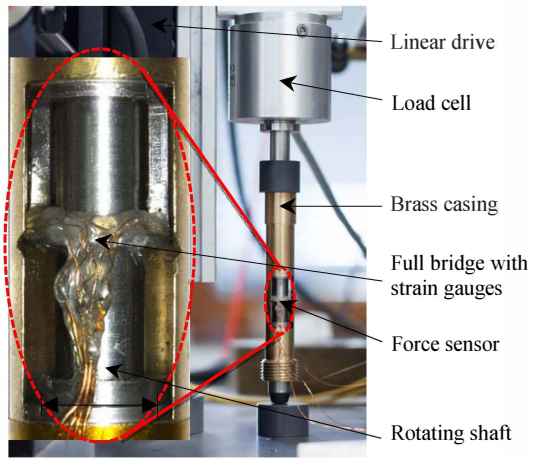

Fig 5. Sensor calibration setup

Additionally, the manufactured force sensor is integrated into the drill brass casing to analyze the force shunt of the friction between the radial bearing and the casing.

Three iterations of each measurement process are executed with steps of 2 N from no load to max 30 N load. The bridge voltage of the sensor is measured with a high impedance voltmeter. Figure 6 shows the average characteristics of the sensor compression tests. The red line shows the slope during compression and relaxation. The black line shows the linear increase of the bridge voltage by loading the sensor with weights.

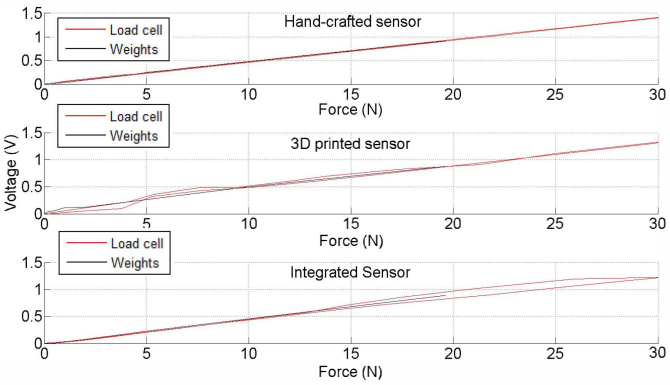

Fig 6. Transient response of the force sensor

The sensor characteristics are summarized in table I with the transmission factor B_0, hysteresis error and linearity error. Once the thrust force exceeds a nominal value of 14 N, friction between the bearing and brass casing results in an increasing hysteresis error.

TABLE I
Sensor Characteristics

Sensor	B_0	Hys	Lin
Hand-crafted	0.047	0.013	0.01
3D Printed	0.045	0.041	0.08
Integrated (<14 N)	0.045	0.020	0.01
Integrated (>14 N)	0.045	0.114	0.03

B. *Thrust force analysis*

Different density of the bone layers lead to a variation of the thrust force signal while drilling with constant feed rate. The sensing of the thrust force signal enables a drilling state recognition to detect different layers while drilling in the bone. Additionally, high friction between the drill tip and bone can be avoided to reduce overheating during cutting operations.

In the following test scenario, several holes are drilled into a test body consisting of 5 mm thick plywood for hard bone layer, 27 mm transitional zone of thick polystyrene for soft bone layer and another layer of plywood. For the test setup, the drill is fixed to the linear drive. Figure 7 shows the thrust force of the 4 mm diameter drill with a drill speed of 7000 rpm and feed rate of 1 mm/s.

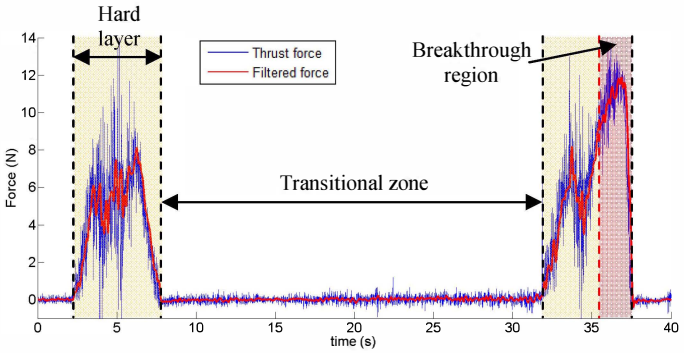

Fig 7. Thrust force during drill procedure

The thrust force signal is filtered with a Butterworth filter of 5th order with the cutoff frequency ω_c = 0.01 rad/s. Once the average thrust force exceeds a threshold of 9.5 N, the drill tip is about to break through the last layer.

CONCLUSION

Freehand bone drilling operations require excellent haptic and visual perception as well as manual skills of the surgeon. A robotic system is capable of supporting the surgeon with additional sensing data to avoid complications during operations and thus improve patient's safety. Based on these requirements, a concept design of a compact surgical drill with an integrated thrust force sensor and active optical marker is introduced. To integrate the sensor in the direct flux of forces of the drill, a hollow cylindrical deformation body is designed. The structural steel element is manufactured through turning and milling as well as low-cost 3D printer technology. The deformation is measured using resistive full-bridge circuit with strain gauges. Sensor characteristics are determined with an automated calibration setup, showing linear behavior and small hysteresis for the occurring measurement range. Several experiments with isokinetic and variable forward speed of the drill were carried out using test bodies with layers of different density properties. The measurement results show a repetitive progress of the thrust force during the drill process in the test body. An excessive increase of the average thrust force is detected before the drill tip breaks through the last layer. The device can be used with the optical tracking system for precise position detection. Additionally, the integration into a robotic positioning system is possible. Further experiments with vertebral bodies are required to obtain appropriate drilling conditions for different bone layer properties.

ACKNOWLEDGMENT

This work is funded by the German Federal Ministry of Education and Research (ref. no. 16SV5773K).

REFERENCES

[1] A. Varma, R. Singh, S. Saraf, and V. Singh, "Pullout strength of misplaced pedicle screws in the thoracic and lumbar vertebrae - A cadaveric study," Indian Journal of Orthopaedics, 2013, 47, 238-243

[2] T. Laine, T. Lund, M. Ylikoski, J. Lohikoski and D. Schlenzka, "Accuracy of pedicle screw insertion with and without computer assistance: a randomised controlled clinical study in 100 consecutive patients", Eur Spine J (2000) 9 :235–240, Springer-Verlag 2000

[3] M. Shoham, S. Brink-Danan, A. Friedlander and N. Knoller, "Bone-Mounted Miniature Robotic System for Spine Surgery," Biomedical Robotics and Biomechatronics, BioRob 2006, pp. 917, 920

[4] P.P. Pott, A. Wagner, A. Köpfle, E. Badreddin, R. Männer, P. Weiser, H.P. Scharf and M. Schwarz, "A handheld surgical manipulator: ITD - Design and first results," 18th international congress and exibition of CARS, Chicago, USA, 23.-26.6.2004

[5] L. Zagorchev and A. Goshtasby, "Surgical robot assistant," Intelligent System Laboratory, Wright State University. Dayton, Ohio. [Online]. Available: http://cecs.wright.edu/~agoshtas/spine.html

[6] G. Boschetti, G. Rosati and A. Rossi, "A haptic system for robotic assisted spine surgery," Conference on Control Applications, pp.19, 24, 28-31 Aug. 2005

[7] G. B. Chung, S. G. Lee, S. Kim, B. Yi, W. Kim, S. M. Oh, Y. S. Kim, J. Park and S. H. Oh, "A robot-assisted surgery system for spinal fusion," International Conference on Intelligent Robots and Systems, pp. 3015, 3021, 2-6 Aug. 2005

[8] Y. Hu, H. Jin, L. Zhang, P. Zhang and J. Zhang, "State Recognition of Pedicle Drilling With Force Sensing in a Robotic Spinal Surgical System," IEEE/ASME Transactions on Mechatronics, pp.1,9

[9] H. Ju, J. Zhang, G. An, X. Pei and G. Xing, "A Robot-Assisted System for Minimally Invasive Spine Surgery of Percutaneous Vertebroplasty Based on CT Images," IEEE Conference on Robotics, Automation and Mechatronics, pp.290,295, 21-24 Sept. 2008

[10] T. Ortmaier, H. Weiss, U. Hagn, M. Grebenstein, M. Nickl, A. Albu-Schaffer, C. Ott, S. Jorg, R. Konietschke, L. Le-Tien and G. Hirzinger, "A hands-on-robot for accurate placement of pedicle screws," IEEE International Conference on Robotics and Automation, pp.4179, 4186, 15-19 May 2006

[11] J. Lee, K. Kim, W. K. Chung, S. Choi and Y. S. Kim, "Human-guided surgical robot system for spinal fusion surgery: CoRASS," IEEE International Conference on Robotics and Automation, pp.3881,3887, 19-23 May 2008

[12] P. Gomes, "Surgical robotics: Reviewing the past, analyzing the present, imagining the future". Robotics and Computer-Integrated Manufacturing, 27, 2011, pp: 261-266.

[13] G. Boiadjiev, T. Boiadjiev, V. Vitkov, K. Delchev,R. Kastelov and K. Zagurski, "Robotized System for Automation of the Drilling in the Orthopedic Surgery. Control Algorithms and Experimental Results". In Proceedings of the 9th IFAC Symp. Robot Control SYROCO '09, pp: 633-638, Gifu, Japan, 2009.

[14] V. Kotev, G. Boiadjiev, H. Kawasaki, T. Mouri, K. Delchev and T. Boiadjiev, "Design of a hand-held robotized module for bone drilling and cutting in orthopedic surgery," IEEE/SICE International Symposium on System Integration (SII), pp.504, 509, 16-18 Dec. 2012

[15] B. Allotta, G. Giacalone and L. Rinaldi, "A hand-held drilling tool for orthopedic surgery," Transactions on Mechatronics, IEEE/ASME, vol.2, no.4, pp.218,229, Dec 1997

[16] JuEun Lee, B. Arda Gozen and O. Burak Ozdoganlar, "Modeling and experimentation of bone drilling forces," Journal of Biomechanics, Volume 45, Issue 6, 5 April 2012